ACS SENSORS

pubs.acs.org/acssensors

Article

Short-Wave Infrared Fluorescence Chemical Sensor for Detection of Otitis Media

Joshua J. Yim,[○] Surya Pratap Singh,[○] Anping Xia, Raana Kashfi-Sadabad, Martina Tholen, David M. Huland, David Zarabanda, Zhixin Cao, Paola Solis-Pazmino, Matthew Bogyo,* and Tulio A. Valdez*

Cite This: *ACS Sens.* 2020, 5, 3411−3419

Read Online

ACCESS | Metrics & More | Article Recommendations

ABSTRACT: Otitis media (OM) or middle ear infection is one of the most common diseases in young children around the world. The diagnosis of OM is currently performed using an otoscope to detect middle ear fluid and inflammatory changes manifested in the tympanic membrane. However, conventional otoscopy cannot visualize across the tympanic membrane or sample middle ear fluid. This can lead to low diagnostic certainty and overdiagnoses of OM. To improve the diagnosis of OM, we have developed a short-wave infrared (SWIR) otoscope in combination with a protease-cleavable biosensor, **6QC-ICG**, which can facilitate the detection of inflammatory proteases in the middle ear with an increase in contrast. **6QC-ICG** is a fluorescently quenched probe, which is activated in the presence of cysteine cathepsin proteases that are up-regulated in inflammatory immune cells. Using a preclinical model and custom-built SWIR otomicroscope in this proof-of-concept study, we successfully demonstrated the feasibility of robustly distinguishing inflamed ears from controls ($p = 0.0006$). The inflamed ears showed an overall signal-to-background ratio of 2.0 with a mean fluorescence of 81 ± 17 AU, while the control ear exhibited a mean fluorescence of 41 ± 11 AU. We envision that these fluorescently quenched probes in conjunction with SWIR imaging tools have the potential to be used as an alternate/adjunct tool for objective diagnosis of OM.

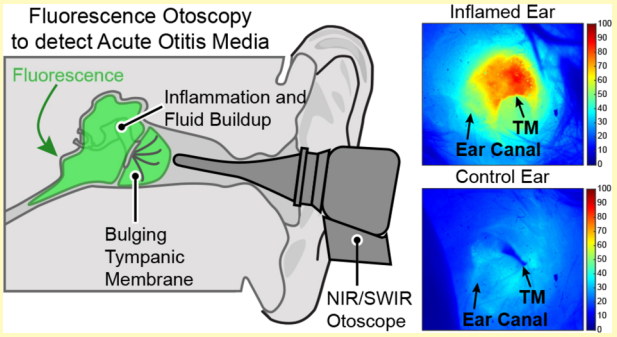

KEYWORDS: *fluorescently quenched probe, protease, short-wave infrared, imaging, otitis media*

Otitis media (OM) is one of the most common reasons for pediatrician visits, antibiotic prescription, and surgery in the pediatric population.[1] Globally, there are over 740 million new cases of OM yearly with the highest incidence rates in children younger than 5 years of age. OM includes a variety of conditions such as acute OM (AOM),[2] OM with effusion (OME), and chronic suppurative OM (CSOM). These conditions are closely related and can overlap, but most importantly, they are linked by the presence of fluid in the middle ear. In the case of CSOM, the fluid drains out of the middle ear through a perforation in the tympanic membrane (TM) or via a tympanostomy tube. While CSOM can be easily discerned due to the presence of ear drainage, otoscopic diagnoses of AOM and OME are not straightforward.[3] The difficulty in identifying the fluid composition in the middle ear is one of the main reasons for OME misdiagnosis[3a4] (Figure 1A).

Visible light pneumatic otoscopy is considered as the best currently available diagnostic tool for OM.[5] However, pneumatic otoscopic examinations suffer from subjective interpretations, especially by unexperienced practitioners.[6] Diagnosis of OME can be challenging and even experienced otolaryngologists need to employ adjuvant diagnostic methods such as otologic microscopy or tympanometry to better discern the presence of middle ear fluid in difficult cases.[7] Some other emerging technologies such as optical coherence tomography, spectral gradient acoustic reflectometry, and sonography have demonstrated immense potential in improving the diagnosis of OM.[8] However, they are yet to be widely adopted, which is primarily due to difficulties in data interpretation and unfamiliarity of the clinicians. Photonic techniques based on fluorescence, Raman spectroscopy, and short-wave infrared (SWIR) spectroscopy constitute another cornerstone in diagnosing OM objectively.[9] Some of our recent efforts have been focused on visualizing middle ear effusion through an otoscope that can detect SWIR wavelengths (1−2 μm) of

Received: June 24, 2020
Accepted: November 2, 2020
Published: November 11, 2020

https://dx.doi.org/10.1021/acssensors.0c01272
ACS Sens. 2020, 5, 3411−3419

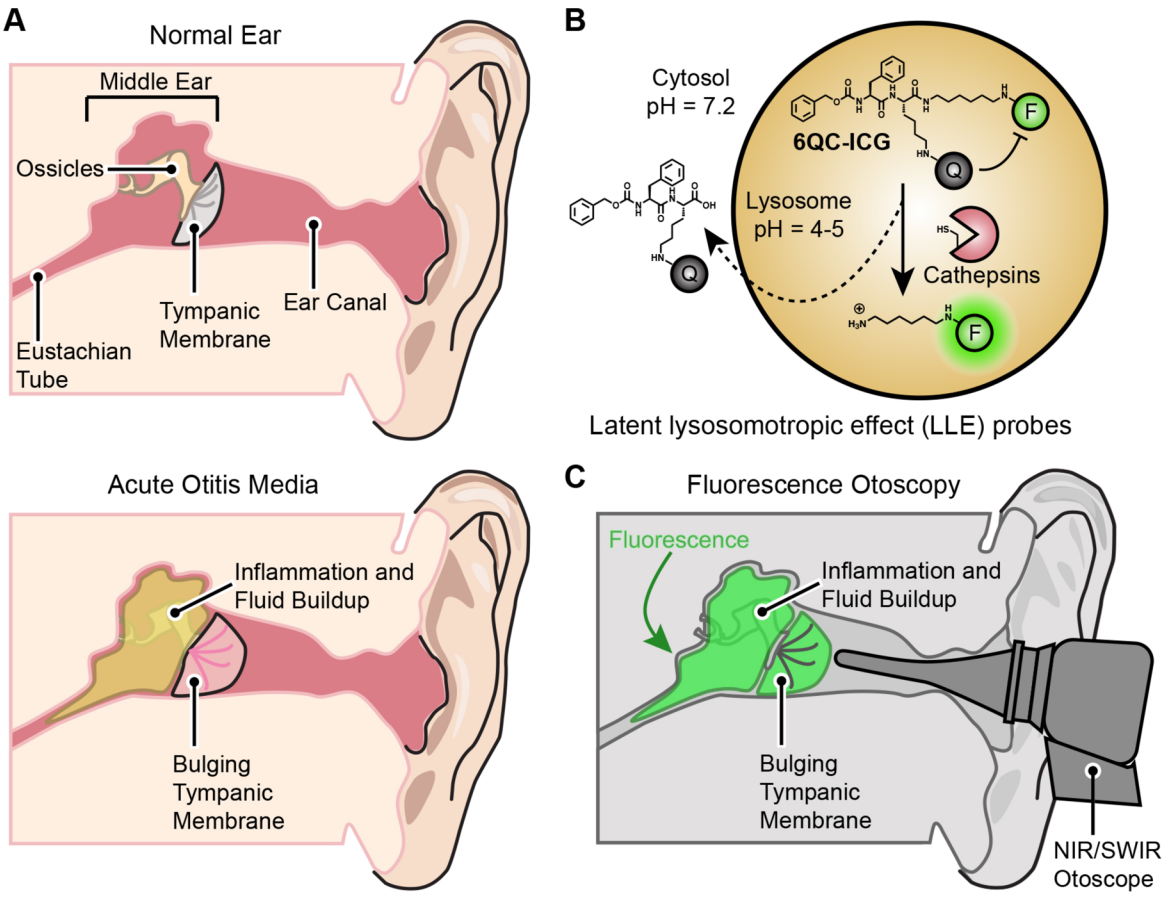

Figure 1. Proposed model for fluorescence-guided detection of OM using an SWIR otoscope. (A) Diagram of normal ear and ear with AOM. (B) Schematic representation of latent lysosomotropic effect, which results in fluorophore retention in the lysosome of substrate probe 6QC upon cleavage by cysteine cathepsins. (C) Schematic of targeted fluorescence otoscopy setup.

light.,[9a10] SWIR otoscopy provides two fundamental advantages over conventional otoscopy. First, it can help in identifying middle ear effusions based on the strong light absorption by middle ear fluid in the SWIR region. Second, due to a longer wavelength, SWIR light can penetrate deeper through tissues, enabling a better view of middle ear structures behind the TM in cases where the fluid is absent.,[9a11] While these studies show great promise in fluid detection, they still lack the ability to sample the composition of the middle ear fluid. To address this challenge, we have looked into employing a fluorescently quenched biosensor that reads out upregulated proteolytic activity associated with OM.[12]

In OM, leukocytes infiltrate the area and release signaling molecules and enzymes that are involved in sustaining inflammation. Among these leukocytes, macrophages play an important role and express various lysosomal proteases such as cysteine cathepsins, matrix metalloproteases, and elastases. These proteases, particularly cathepsin B, have been shown to play an important role in OME.[12a] Therefore, targeting upregulated cathepsins during OM-associated inflammation may be an effective approach to identify OM. To detect cathepsin activity, we used **6QC-ICG**, a fluorescently quenched substrate probe that broadly reads out the proteolytic activity of cysteine cathepsins.[13] This probe consists of a short peptide sequence Cbz-Phe-Lys. The quencher is attached to the lysine sidechain, and an FDA-approved indocyanine green (ICG) dye is conjugated to the lysine through a 6-carbon linker. It has shown potential for use in surgical resection of tumor malignancies with high sensitivity and specificity.[13a] **6QC-ICG** is able to amplify the proteolytic signal due to a high cleavage turnover rate, accumulating in the site of inflammation by exploiting the latent lysosomotropic effect (Figure 1B). The optically dark probe releases its quencher upon cathepsin recognition and cleavage in the lysosomes. When the peptide bond is cleaved, the fluorophore fragment containing a primary amine becomes protonated in the acidic environment of the lysosome and leads to its lysosomal accumulation, promoting cellular retention of the fluorophore (Figure 1B). Its ability to read out broad-cathepsin activity with a near-infrared (NIR) and SWIR-compatible ICG fluorophore makes it an ideal candidate for detecting OM (Figure 1C). In this study, using **6QC-ICG** and various NIR imagers, we demonstrate the feasibility of distinguishing inflamed ears from normal ears in a mouse model of OM. Furthermore, we custom-designed a preclinical fluorescence SWIR otomicroscope to detect the activation of **6QC-ICG** *in vivo*. Overall, our findings support prospective application of optical contrast agents in accurately identifying OM.

RESULTS AND DISCUSSION

***In Vivo* Detection of OM Using a 6QC-ICG Probe with an NIR Fluorescence Imager.** To evaluate **6QC-ICG** for the detection of OM, we used a recently established OM mouse model based on lipopolysaccharide (LPS) treatment.[9b] LPS, a major component of the outer membrane in most Gram-negative bacteria, is a powerful mediator of inflammatory

https://dx.doi.org/10.1021/acssensors.0c01272
ACS Sens. 2020, 5, 3411−3419

responses and is a widely accepted agent to induce OM in mice.[14] Several studies have shown that LPS treatment in the ear of mice causes functional and structural changes similar to those in the early stages of clinical OM.[15] Additionally, LPS is known to activate macrophages that cause release of inflammatory cytokines.,[15a,15c,15d] With the LPS-induced mouse model of OM, we first evaluated the ability of **6QC-ICG** to identify OM using the Pearl Trilogy imaging system—an 800 nm NIR wide-field imager.[9b] Since the ICG fluorophore in **6QC-ICG** has a long emission range (750–950 nm), we conducted initial studies by employing commercially available NIR (~800 nm) fluorescence imagers. In animals treated with **6QC-ICG** via tail vein injection, a fluorescence signal developed over a period of 24 h as the NIR fluorescence accumulated and facilitated clear differentiation between the inflamed and control ears (Figure 2A). We also evaluated the efficacy of an FDA-approved NIR fluorescent dye, ICG, to investigate if it could differentiate between the inflamed and healthy ears. ICG, being the same fluorophore employed in **6QC-ICG**, serves as an ideal internal control to provide a readout of potential dye accumulation due to generic uptake in the accumulated fluid or at the inflammation site. However, the free ICG dye alone did not discriminate between the inflamed and healthy ears at any time point over the course of 24 h (Figure 2A,B). Furthermore, the ICG dye was excreted from the mouse, and the fluorescence signal was quickly depleted. In contrast, quantification of the **6QC-ICG** probe signal revealed that the inflamed ear had a statistically significant increase in the mean fluorescence intensity with respect to the untreated right ear (0.18 ± 0.05 AU vs 0.14 ± 0.03 AU; p = 0.005; Figure 2C). The mean signal-to-background ratio (SBR) of the inflamed left ear was 1.3 at 24 h (Figure 2C). These results provided initial evidence in support of visualizing and differentiating inflammation in the ears through imaging of the **6QC-ICG** signal.

The ability of **6QC-ICG** to identify OM objectively was further confirmed by analyzing the fluorescence signal from excised middle and inner ear tissues. While the live animal imaging of the whole mouse revealed higher fluorescence intensity from the inflamed ears, signal variations due to the external ear could not be completely ignored. Therefore, in the next step, we isolated ear tissues consisting of both middle and inner ears for further imaging studies. Fluorescence images of ear tissues were acquired using the same 800 nm wide-field imager used for the live animal imaging (Figure 3A). We observed a statistically significant (p = 0.0013) increase in the overall fluorescence signal in the LPS-treated ear tissues (0.37 ± 0.14 AU) with respect to the control (0.18 ± 0.08 AU) with a mean SBR of 2.1 (Figure 3B). As observed in the live animal imaging studies, the mice injected with only the ICG dye did not show any difference at 24 h post injection (Figure 3B). These results confirmed the data obtained from the live animal imaging studies and verified that the statistically significant accumulation of fluorescence signals only occurred in the inflamed ear.

Evaluation of 6QC-ICG Fluorescence Accumulation in Ear Tissue Sections. To confirm the precise location of fluorescence signals originating from the **6QC-ICG** probe in the ear, we obtained 10 μm-thick serial histological sections and scanned them using a flatbed NIRF scanner. As mentioned, **6QC-ICG** contains a fluorophore reporter, which contains a primary amine that gets protonated in the lysosomes after probe cleavage. This allows the fluorescence signal to be retained in the macrophages at the site of inflammation. This retention of signal allows us to perform direct fluorescence scans of the tissue sections for visualizing the location of the

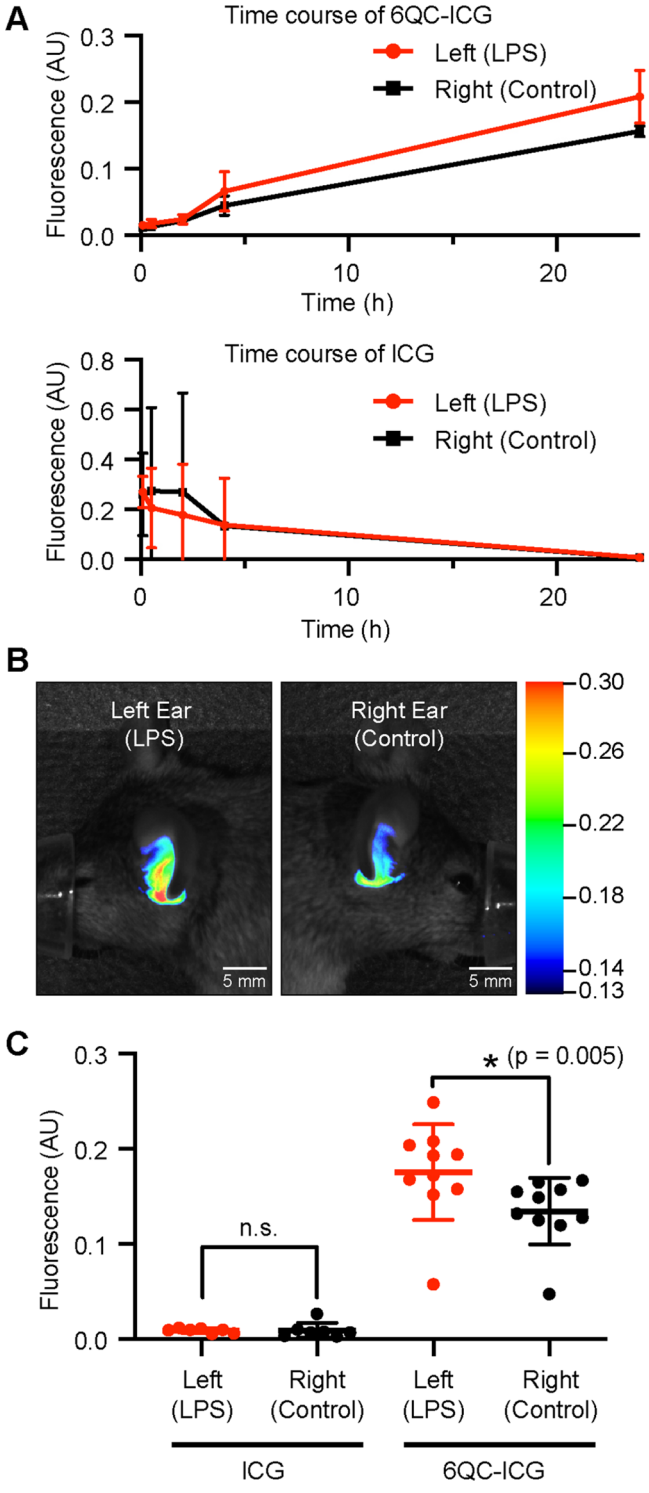

Figure 2. NIR fluorescence imaging of murine ear inflammation using **6QC-ICG** and ICG. (A) Time course of fluorescence over 24 h for mice ears injected with either **6QC-ICG** (top) or ICG (bottom). (B) Image of a mouse treated with LPS (left ear) and left untreated (right ear) followed by **6QC-ICG** injection via tail vein and imaging after 24 h using an 800 nm wide-field imager (LI-COR Pearl Trilogy). (C) Quantification of fluorescence of mouse ears injected with either **6QC-ICG** or ICG (24 h post injection, n = 11).

https://dx.doi.org/10.1021/acssensors.0c01272
ACS Sens. 2020, 5, 3411−3419

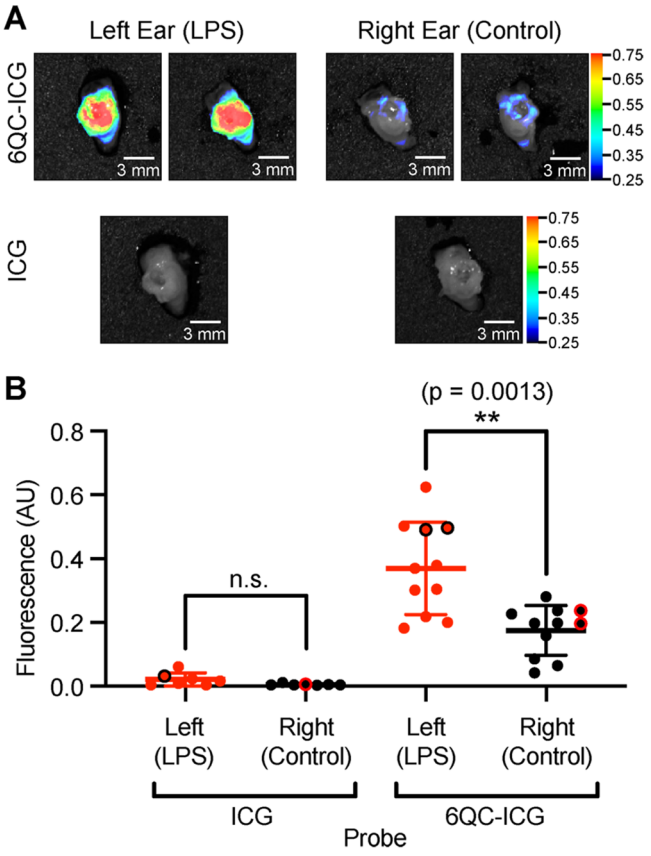

Figure 3. NIR fluorescence imaging of excised ear tissue using **6QC-ICG** and ICG. (A) Representative images of middle and inner ear specimens from mice treated with LPS (left ear) and control (right ear) injected with **6QC-ICG** or ICG and imaged after 24 h using a 800 nm wide-field imager (LI-COR Pearl Trilogy). (B) Fluorescence quantification of the excised right and left ear tissue from mice injected with **6QC-ICG** or ICG (2.3 mg/kg, 24 h post injection (PI), $n = 11$). Highlighted dots correspond to the images presented in (A).

probe signal. Fluorescence scans were directly compared with adjacent H&E-stained sections to establish a physiological context. We observed that the increased fluorescence signal originates primarily from the TM and middle ear mucosa (Figure 4A). The TM is disrupted in the left ear as LPS was administered in a trans-tympanic manner (Figure 4A), denoted by a red asterisk in the H&E image. Thickening of the TM and mucosa from LPS injection and inflammation were visible in the LPS-treated left ear. Increased accumulation of fluorescence signal was observed in the TM and mucosa. In the healthy right ear, fluorescence accumulation was not observed in the TM or mucosa. With **6QC-ICG**, the mean SBR of 3.8 was observed. Mean fluorescence values of the inflamed and control ears were 7.6 ± 2.8 and 2.0 ± 1.2 AU, respectively (Figure 4B). Enhancement in the number of macrophages and cathepsin expression in LPS-treated ear was confirmed by immunostaining using cathepsin B and CD68 antibodies (Figure 4C). The significant difference ($p < 0.0001$) between the LPS-treated and untreated ears suggests that **6QC-ICG** signal accumulation in the middle ear can facilitate objective identification of ear inflammation.

SWIR Fluorescence Otoscopy Allows Visualization of AOM Using 6QC-ICG in Mouse Models. SWIR imaging has significant advantages over NIR due to minimized scattering, decreased autofluorescence, and higher penetration depth. Most importantly, it exhibits high water absorption, allowing detection of ear effusions.[9a] We hypothesize that fluorescence properties of **6QC-ICG**, particularly ICG fluorophore, can be detected in the SWIR region and may be utilized for determining the presence of inflammation based on the protease signature of middle ear fluid. Therefore, we custom-designed an SWIR fluorescence otomicroscope and used it for *in vivo* visualization of inflammation in the ear (Figure 5A,B). Similar to routinely employed clinical otoscopes, we used a specially designed "speculum" to deliver light effectively inside the ear cavity. The speculum also helped reduce signal losses from the external ear (Figure 5A,B). The efficacy of the long-pass filter in removing interfering reflected laser light was established through imaging of a reflective surface under similar conditions.

Our findings suggest that the presence of inflammation in the ear is easily distinguishable using this setup (Figure 5C). Fluorescence quantification of a group of six animals revealed strong fluorescence signals originating from the TM (Figure 5C). A statistically significant difference ($p = 0.0006$) in signal intensities between the inflamed left ear and control right ear was observed at 24 h (mean fluorescence of 81 ± 17 AU in LPS-injected ear, 41 ± 11 in control; $p = 0.0006$) with an overall SBR of 2.0 (Figure 5D). Fluorescence SBR values obtained from *in vivo* SWIR imaging (SBR = 2.0) were similar to those obtained using *ex vivo* NIR imaging of the excised middle ear tissue (SBR = 2.1). This shows that **6QC-ICG** with SWIR imaging facilitates a more robust detection of ear inflammation in live animals as compared to *in vivo* NIR imaging (SBR = 1.3) along with minimal background signals.

DISCUSSION

OM is characterized by the presence of fluid in the middle ear. Failure to diagnose OM can result in severe complications including facial nerve palsy, meningitis, permanent hearing loss, and brain abscesses. Consequently, there is a pressing clinical need for a more accurate and noninvasive method for sampling the middle ear fluid without disrupting the TM. Recent studies have demonstrated that SWIR otoscopy can facilitate visualization of fluid behind the TM.,[9a10] However, SWIR otoscopy has some limitations as it cannot determine the fluid composition.

In this study, we evaluated a cathepsin-activated fluorescence substrate probe, **6QC-ICG**, in combination with a custom-designed SWIR fluorescence otomicroscope to achieve detection of ear inflammation in a murine model of OM. LPS treatment in the middle ear is known to enhance the infiltration of macrophages, leukocytes, and monocytes.[9b,15b] It also induces the release of inflammatory cytokines such as interleukin-1 (IL-1) and IL-3.[15b] We demonstrated that upregulated cathepsin protease activity in inflammation-associated macrophages can be successfully utilized for imaging inflammation using the **6QC-ICG** probe. Accumulation of fluorescence signals in the LPS-injected left ear post systemic administration of the probe provided evidence of cleavage by proteases, which were later verified on excised ear specimens (Figures 2 and 3). Previous studies have shown that LPS-induced effects in the TM are primarily manifested in the form of increased TM thickness, infiltration of inflammatory cells, and collagen rearrangement.[9b,15e,16] Our study corroborated these observations as most of the detected fluorescence originated from the thickened TM and middle ear mucosa of LPS-injected ears (Figure 4).

https://dx.doi.org/10.1021/acssensors.0c01272
ACS Sens. 2020, 5, 3411−3419

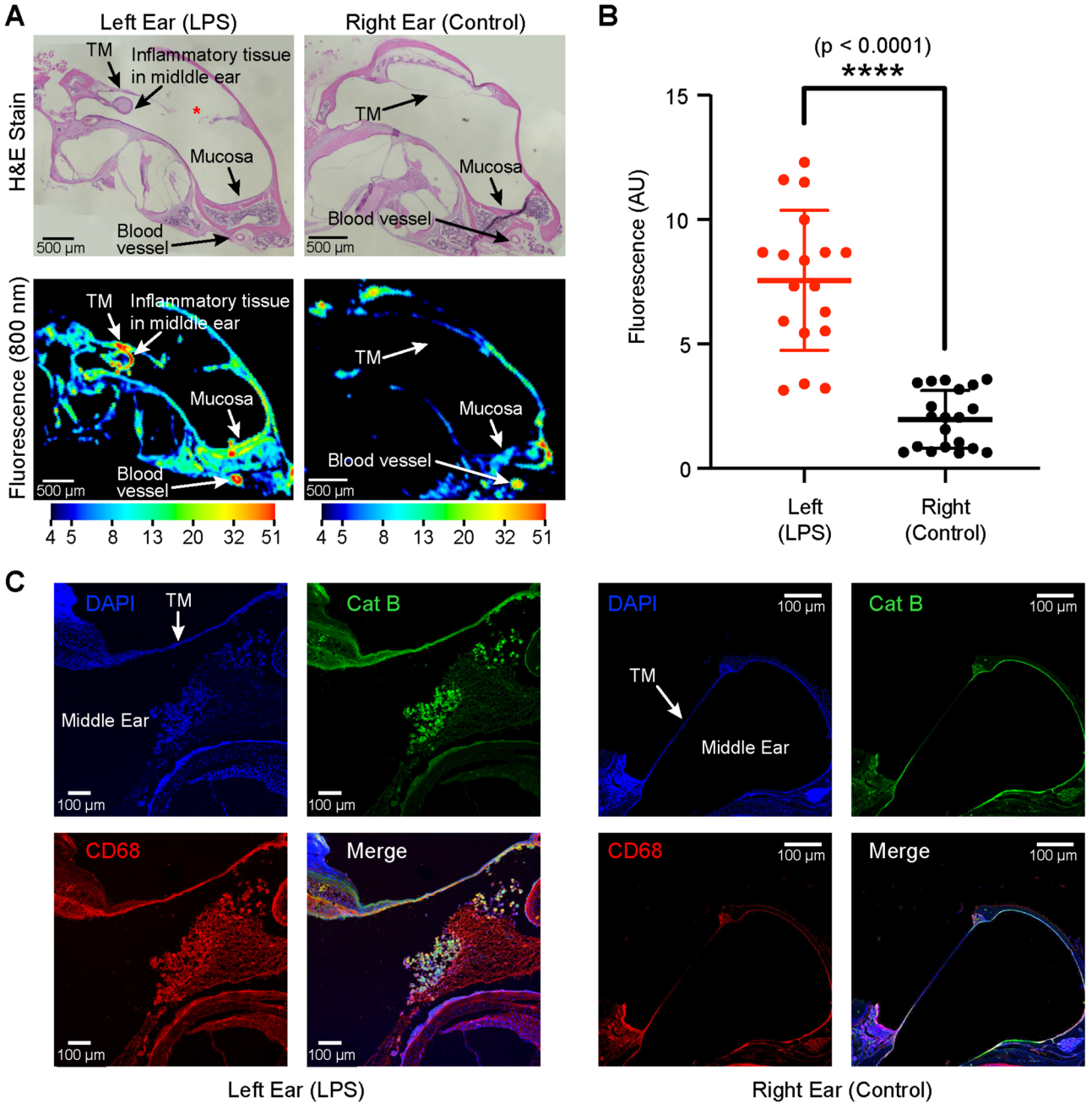

Figure 4. NIR fluorescence imaging of ear tissue sections. (A) Representative histological sections of ears (left: LPS-injected; right: untreated) taken from mice injected with **6QC-ICG** and imaged at 24 h. Top row shows H&E-stained and bottom row shows fluorescence of corresponding unstained tissue sections. The slides were scanned on an 800 nm NIR flatbed scanner (LI-COR Odyssey CLx). The red asterisk denotes torn TM. (B) Fluorescence quantification of unstained ear tissue sections from mice injected with **6QC-ICG** (2.3 mg/kg, 24 h PI). (C) Confocal images of the tympanic membrane and middle ear mucosa of LPS-treated (left) and untreated (right) mice (10× magnification). Cathepsin B imaged with anti-cathepsin B antibody (green) and macrophage infiltration imaged with anti-CD68 antibody (red).

6QC-ICG is a "turn-on" fluorescent probe that is activated by upregulated cathepsin protease activity in macrophages associated with inflammation. Since the fluorescence signal is only activated by cathepsins and is not active when the probe is intact and quenched, the contrast is improved, and an additional washout step often associated with contrast dyes is not required. Compared to ICG dye alone, the lysosomotropic effect further allows the postcleaved portion of the **6QC-ICG** probe to accumulate in the lysosomes of the macrophages and prevents the dye from diffusing out of the cells. The lysosomotropic effect could be observed while comparing the 24 h time course of the probes, where ICG fluorescence quickly diminished, while **6QC-ICG** fluorescence increased with time to provide contrast between the left and right ears.

NIR imaging, in combination with exogenous fluorophores, has been extensively employed for visualizing cancer margins and vasculature during intraoperative procedures. However, they have not been widely explored for other clinical applications such as infectious processes. One of the major hindrances in translating these observations to a noninvasive medical device is the limited penetration depth of standard optical imaging methods.,[11b17] Imaging in the SWIR range can

https://dx.doi.org/10.1021/acssensors.0c01272
ACS Sens. 2020, 5, 3411−3419

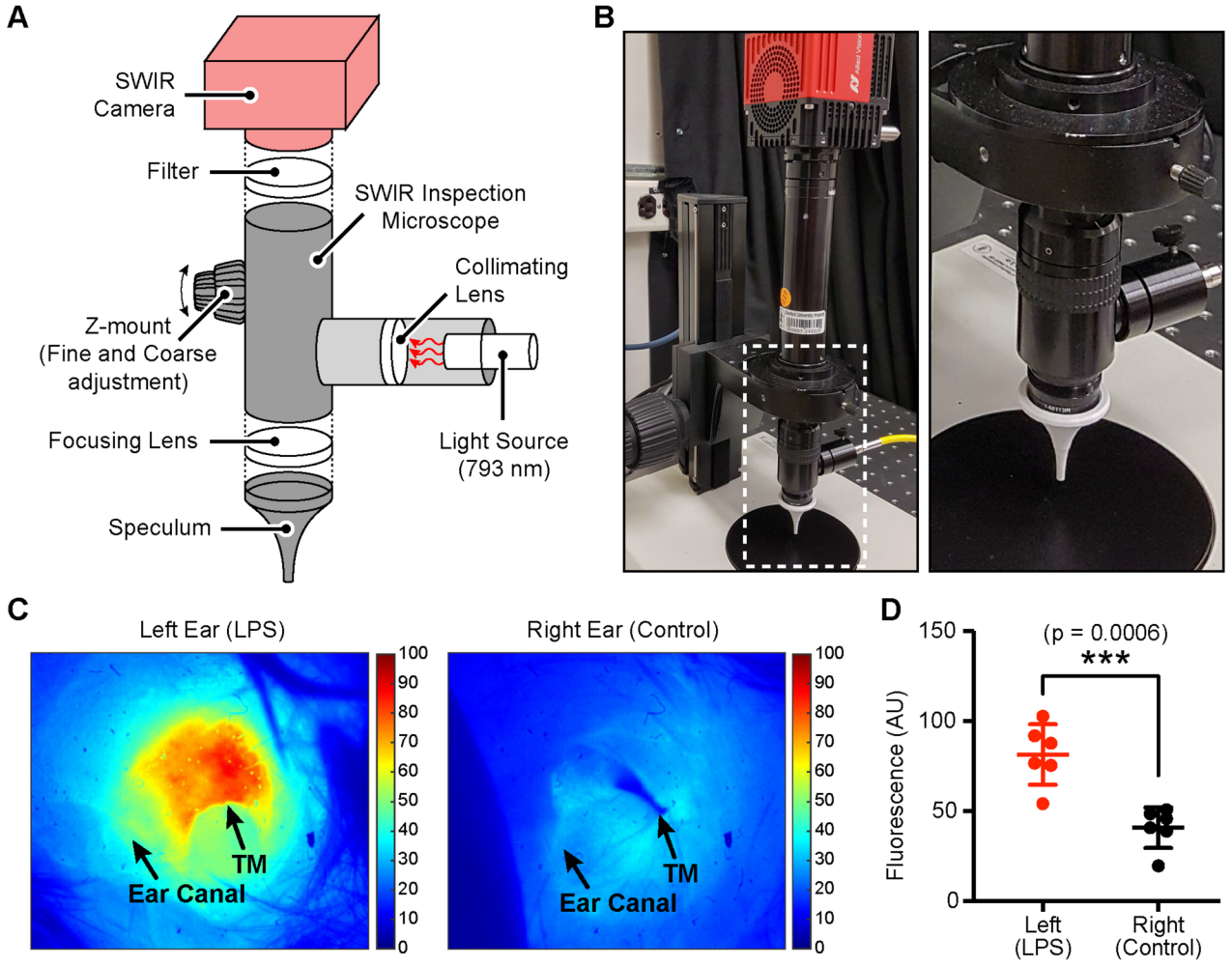

Figure 5. *In vivo* SWIR otomicroscopy imaging of ear inflammation. (A) Diagram of the custom-designed SWIR otomicroscope setup. (B) Image of SWIR otomicroscope (left) and closeup of 3D-printed and fitted speculum (right) used for *in vivo* imaging. (C) Fluorescence from the left ear (LPS injected) and right ear (untreated) of animals injected with **6QC-ICG** (24 h) by an SWIR otomicroscope (793 nm laser, 808 nm long-pass filter, SWIR camera). (D) Quantification of mean fluorescence for the TM region of interest in the middle ear (n = 6).

provide improved visualization of deeper structures as compared to NIR imaging.[11a11b11c] As mentioned before, we recently developed an SWIR otoscope for diagnosing OM in pediatric populations. A large-scale clinical trial is currently underway to evaluate its efficacy in detecting fluid in the middle ear.[10] In addition to enhancing diagnostic capabilities, the main benefit of the SWIR otoscope is the ability to be integrated readily in the current OM management framework. Utilizing a **6QC-ICG** probe along with an SWIR otoscope is based on the fact that ICG fluorophore has a long tail in the SWIR region, which can be detected by our SWIR otoscope.[18] Our custom-designed preclinical fluorescence otomicroscope provided evidence that *in vivo* visualization of **6QC-ICG** at the inflamed sites in the ear is possible (Figure 5). Additional animal studies focusing on probe delivery, dosing, timing, and ototoxicity of the compound are required to evaluate the true clinical potential of the **6QC-ICG** probe. In this study, the probe was administered intravenously, which is clinically suboptimal for pediatric populations for a common medical issue. Studies into various formulation methods, including oral administration and application in the form of eardrops, still need to be evaluated. We envision that protease-cleavable fluorescent biosensors in combination with SWIR detection devices can also be effective in diagnosing other infectious diseases in pediatric patients, where the use of ionizing radiation techniques is not ideal. Any infectious process that elicits an inflammatory response with the associated increase in proteolytic activity, such as cervical abscesses, could be detected using this approach.

■ CONCLUSIONS

Overall, this study demonstrates that the use of fluorescence probes with SWIR otoscopy has the potential to improve the overall diagnosis of OM. The ability to simultaneously determine fluid presence and composition using the SWIR otoscope and **6QC-ICG** can serve as a powerful tool that could enable improved tracking of AOM and CSOM treatment and follow-ups. In addition to OM, ear conditions such as mastoiditis and cholesteatoma also lack objective diagnostic tools. Since these ear conditions also have chronic inflammation, we anticipate that probes such as **6QC-ICG** could also be used to image these ear conditions. While more work needs to be done to formulate the probe for routine clinical use, we envision that **6QC-ICG** can be used as an objective diagnostic test, which may aid physicians in their treatment decisions, ultimately yielding better clinical outcomes.

https://dx.doi.org/10.1021/acssensors.0c01272
ACS Sens. 2020, 5, 3411−3419

MATERIALS AND METHODS

Compound Synthesis. Synthetic procedure and characterization of **6QC-ICG** are outlined by Yim et al.[13a] All reagents and materials used in the synthesis of **6QC-ICG** were obtained from commercial sources and used without further purification. IRDye QC-1 NHS ester was obtained from LI-COR Biosciences (Lincoln, NE, USA) and ICG-NHS ester was from Intrace Medical (Lausanne, Switzerland). Compounds were synthesized using reported procedures and purified by reverse-phase preparative HPLC.

OM Mouse Model. *In vivo* studies of murine models were conducted according to the current NIH and Stanford University Institutional Animal Care and Use Committee (IACUC) guidelines (APLAC #33028). A total of 22 female C57BL/6J mice (aged 4−6 weeks) were purchased from Jackson Laboratory (Bar Harbor, ME, USA). Mice were anesthetized with a standard dose of ketamine and xylazine mixture. *Salmonella enterica*-derived lipopolysaccharide (LPS; L7261, Sigma) emulsion was prepared in normal saline (0.9%) at a stock concentration of 20 mg/mL. The left ear was treated with 3 μL of LPS through a trans-tympanic injection under a microscopic view. The right ear remained untreated and served as a control.

Probe Administration. Stocks (10 mM) of either **6QC-ICG** or indocyanine green (ICG) were dissolved in a solution of 10% DMSO prepared in 100 μL of phosphate-buffered saline (PBS) to a final concentration of 25 nmol per injection. It was administered intravenously through mouse tail vein and imaged between 1 and 24 h post injection.

Wide-Field Near-Infrared Fluorescence (NIRF) Imaging. Mice were imaged after 24 h of probe injection using the Pearl Trilogy Small Animal Imaging System (LI-COR Biosciences, Lincoln, NE, USA) while being kept under anesthesia with 2% (v/v) isoflurane (Fluriso, VetOne, Boise, ID, USA). Signal was detected using the 800 nm filter set. Images were analyzed using Image Studio Software (LI-COR Biosciences, Lincoln, NE, USA).

SWIR Fluorescence Otoscopic Detection of OM. SWIR fluorescence otoscopy was performed after 24 h of **6QC-ICG** probe treatment using a custom-built imaging system equipped with a fiber (200 μm core)-coupled 793 nm laser (20 W, Lumics LU0793D140-D10DH) and Allied Vision Goldeye G-032 Cool TEC2 camera (Figure 5). The sensor set point of the camera was at −30 °C. The laser light excitation was guided to the animal ear through a lens and specially designed speculum (3D-printed using poly-lactic acid). Epifluorescence was collected via a high-efficiency long-pass filter (BlP01-808R-25, Semrock) before reaching the camera. The average excitation flux at the site of delivery was ∼25−30 mW cm^{-2}. The assembly was partially enclosed, and experiments were performed in a dark environment to avoid exposure to unwanted light. The images were acquired using a platform-independent Vimba SDK (Allied Vision) with a uniform acquisition time of 10 s. During the imaging, anesthetized mice were placed over a predefined heated platform in the left and right lateral decubitus position to acquire images from the right and left ears, respectively. MATLAB programming environment was used for processing and analysis of the acquired images.

Histology. Following otoscopy, animals under deep anesthesia were euthanized via cervical dislocation. Both the middle and inner ears were harvested. The tissues were fixed in 4% paraformaldehyde (PFA) overnight at 4 °C and rinsed with phosphate-buffered saline (PBS) of pH 7.3 to remove the residual traces of PFA. This was followed by 48 h decalcification of samples using 0.5 M EDTA. Tissues were rinsed free of any EDTA solution by multiple washes using PBS followed by overnight incubation in 30% sucrose at 4 °C. In the end, tissues were processed through serial incubation in sucrose and OCT compound (Fisher Scientific) mixture. Tissue sections (10 μm) were obtained from OCT blocks and either stained with hematoxylin and eosin (H&E) or analyzed without staining by NIRF scanning.

Flatbed Near-Infrared Fluorescence (NIRF) Scanning of Slides. H&E-stained slides and unstained cryosections were placed directly on the Odyssey CLx imaging system (LI-COR Biosciences, Lincoln, NE, USA) and imaged using the following parameters: channel, 800 nm; resolution, 21 μm; intensity, auto; quality, highest. Images were analyzed using Image Studio Software (LI-COR Biosciences, Lincoln, NE, USA).

Immunofluorescence. Frozen ear samples in OCT blocks were sectioned into 10 μm slices, fixed with 4% PFA for 30 min, and washed three times with PBS. Blocking buffer (PBS + 0.3% Tx-100) was then added on top of the sections and left for 2 h at room temperature. Subsequently, sections were incubated with primary mouse anti-cathepsin B (AF965; R&D Systems, Minneapolis, MN, USA) and recombinant anti-CD68 antibody (ab213363, Abcam, Cambridge, MA, USA). After 24 h, sections were incubated with secondary antibodies for 1 h at room temperature. The tissues were nuclear-stained with DAPI (ab104139) in mounting medium and covered with a cover slip.

Confocal Microscopy. A confocal laser scanning microscope (CLSM700, Zeiss) was used to image tissues using a 10× objective. Images were processed with ImageJ software.

Statistical Analysis. Statistical analysis was performed in Excel (Microsoft, Redmond, WA, USA) and Prism (GraphPad Software, San Diego, CA, USA). The signal-to-background ratio (SBR) was calculated as described in the figure legends. Unless otherwise noted, all values in figures are presented as mean ± SD. Statistical significance was calculated based on the Student's *t*-test (two-tailed, unpaired).

AUTHOR INFORMATION

Corresponding Authors

Matthew Bogyo − *Department of Chemical and Systems Biology, Department of Pathology, and Department of Microbiology and Immunology, Stanford University School of Medicine, Stanford, California 94305, United States;* orcid.org/0000-0003-3753-4412; Email: mbogyo@stanford.edu

Tulio A. Valdez − *Department of Otolaryngology−Head & Neck Surgery Divisions, Stanford University School of Medicine, Stanford, California 94305, United States;* Email: tvaldez1@stanford.edu

Authors

Joshua J. Yim − *Department of Chemical and Systems Biology, Stanford University School of Medicine, Stanford, California 94305, United States*

Surya Pratap Singh − *Department of Otolaryngology−Head & Neck Surgery Divisions, Stanford University School of Medicine, Stanford, California 94305, United States; Department of Biosciences and Bioengineering, Indian Institute of Technology Dharwad, Dharwad, Karnataka 580011, India;* orcid.org/0000-0001-9984-5385

Anping Xia − *Department of Otolaryngology−Head & Neck Surgery Divisions, Stanford University School of Medicine, Stanford, California 94305, United States*

Raana Kashfi-Sadabad − *Department of Otolaryngology−Head & Neck Surgery Divisions, Stanford University School of Medicine, Stanford, California 94305, United States*

Martina Tholen − *Department of Pathology, Stanford University School of Medicine, Stanford, California 94305, United States*

David M. Huland − *Molecular Imaging Program at Stanford, Department of Radiology, Stanford University School of Medicine, Stanford, California 94305, United States*

David Zarabanda − *Department of Otolaryngology−Head & Neck Surgery Divisions, Stanford University School of Medicine, Stanford, California 94305, United States*

https://dx.doi.org/10.1021/acssensors.0c01272
ACS Sens. 2020, 5, 3411−3419

Zhixin Cao − *Department of Otolaryngology−Head & Neck Surgery Divisions, Stanford University School of Medicine, Stanford, California 94305, United States; Department of Pathology, Shandong Provincial Hospital Affiliated to Shandong First Medical University, Jinan, Shandong 250021, China*

Paola Solis-Pazmino − *Department of Otolaryngology−Head & Neck Surgery Divisions, Stanford University School of Medicine, Stanford, California 94305, United States*

Complete contact information is available at: https://pubs.acs.org/10.1021/acssensors.0c01272

Author Contributions

○J.J.Y. and S.P.S. contributed equally to this work.

Author Contributions

All authors have given approval to the final version of the manuscript.

Notes

The authors declare no competing financial interest.

■ ACKNOWLEDGMENTS

This work was supported in part by the following grants: R01 EB028628 and R01 EB005011 (to M.B.), Stanford ChEM-H Chemistry/Biology Interface Predoctoral Training Program and NSF Graduate Research Fellowship grant DGE-114747 (to J.J.Y.), NCI training grant T32-CA118681 (to D.M.H.), and Shandong Provincial Key Research and Development Program no. 2019GSF108268 (to Z.C.). The authors thank N. van den Berg in the Rosenthal laboratory for generously assisting with NIRF image scanning. Help from J. A. Vargas for 3D printing of the otoscope speculum and C. Faniku for immunofluorescence experiments is gratefully acknowledged.

■ ABBREVIATIONS

OM, otitis media; AOM, acute otitis media; OME, otitis media with effusion; CSOM, chronic suppurative otitis media; SWIR, short-wave infrared; NIR, near-infrared; ICG, indocyanine green; SBR, signal-to-background ratio; LPS, lipopolysaccharide; TM, tympanic membrane

■ REFERENCES

(1) Rovers, M. M.; Schilder, A. G.; Zielhuis, G. A.; Rosenfeld, R. M. Otitis media. *Lancet* **2004**, *363*, 465−473.

(2) Lieberthal, A. S.; Carroll, A. E.; Chonmaitree, T.; Ganiats, T. G.; Hoberman, A.; Jackson, M. A.; Joffe, M. D.; Miller, D. T.; Rosenfeld, R. M.; Sevilla, X. D.; Schwartz, R. H.; Thomas, P. A.; Tunkel, D. E. The diagnosis and management of acute otitis media. *Pediatrics* **2013**, *131*, e964−e999.

(3) (a) Pichichero, M. E.; Poole, M. D. Assessing diagnostic accuracy and tympanocentesis skills in the management of otitis media. *Arch. Pediatr. Adolesc. Med.* **2001**, *155*, 1137−1142. (b) Verhoeff, M.; van der Veen, E. L.; Rovers, M. M.; Sanders, E. A. M.; Schilder, A. G. M. Chronic suppurative otitis media: a review. *Int. J. Pediatr. Otorhinolaryngol.* **2006**, *70*, 1−12.

(4) Rosenfeld, R. M. Diagnostic certainty for acute otitis media. *Int. J. Pediatr. Otorhinolaryngol.* **2002**, *64*, 89−95.

(5) (a) Rosenfeld, R. M.; Shin, J. J.; Schwartz, S. R.; Coggins, R.; Gagnon, L.; Hackell, J. M.; Hoelting, D.; Hunter, L. L.; Kummer, A. W.; Payne, S. C.; Poe, D. S.; Veling, M.; Vila, P. M.; Walsh, S. A.; Corrigan, M. D. Clinical Practice Guideline: Otitis Media with Effusion (Update). *Otolaryngol. Head Neck Surg.* **2016**, *154*, S1−S41. (b) Takata, G. S.; Chan, L. S.; Morphew, T.; Mangione-Smith, R.; Morton, S. C.; Shekelle, P. Evidence assessment of the accuracy of methods of diagnosing middle ear effusion in children with otitis media with effusion. *Pediatrics* **2003**, *112*, 1379−1387.

(6) (a) MacClements, J. E.; Parchman, M.; Passmore, C. Otitis media in children: use of diagnostic tools by family practice residents. *Fam. Med.* **2002**, *34*, 598−603. (b) Ouedraogo, E.; Labrecque, M.; Cote, L.; Charbonneau, K.; Legare, F. Use and teaching of pneumatic otoscopy in a family medicine residency program. *Can. Fam. Physician* **2013**, *59*, 972−979.

(7) (a) Rogers, D. J.; Boseley, M. E.; Adams, M. T.; Makowski, R. L.; Hohman, M. H. Prospective comparison of handheld pneumatic otoscopy, binocular microscopy, and tympanometry in identifying middle ear effusions in children. *Int. J. Pediatr. Otorhinolaryngol.* **2010**, *74*, 1140−1143. (b) Lee, D. H. How to improve the accuracy of diagnosing otitis media with effusion in a pediatric population. *Int. J. Pediatr. Otorhinolaryngol.* **2010**, *74*, 151−153. (c) Abbott, P.; Rosenkranz, S.; Hu, W.; Gunasekera, H.; Reath, J. The effect and acceptability of tympanometry and pneumatic otoscopy in general practitioner diagnosis and management of childhood ear disease. *BMC Fam. Pract.* **2014**, *15*, 181.

(8) (a) Linden, H.; Teppo, H.; Revonta, M. Spectral gradient acoustic reflectometry in the diagnosis of middle-ear fluid in children. *Eur. Arch. Oto-Rhino-Laryngol.* **2007**, *264*, 477−481. (b) Monroy, G. L.; Pande, P.; Nolan, R. M.; Shelton, R. L.; Porter, R. G.; Novak, M. A.; Spillman, D. R.; Chaney, E. J.; McCormick, D. T.; Boppart, S. A. Noninvasive in vivo optical coherence tomography tracking of chronic otitis media in pediatric subjects after surgical intervention. *J. Biomed. Opt.* **2017**, *22*, 1−11. (c) Monroy, G. L.; Pande, P.; Shelton, R. L.; Nolan, R. M.; Spillman, D. R., Jr.; Porter, R. G.; Novak, M. A.; Boppart, S. A. Non-invasive optical assessment of viscosity of middle ear effusions in otitis media. *J. Biophotonics* **2017**, *10*, 394−403. (d) Monroy, G. L.; Won, J.; Spillman, D. R., Jr.; Dsouza, R.; Boppart, S. A. Clinical translation of handheld optical coherence tomography: practical considerations and recent advancements. *J. Biomed. Opt.* **2017**, *22*, 1−30. (e) Nguyen, C. T.; Jung, W.; Kim, J.; Chaney, E. J.; Novak, M.; Stewart, C. N.; Boppart, S. A. Noninvasive in vivo optical detection of biofilm in the human middle ear. *Proc. Natl. Acad. Sci. U. S. A.* **2012**, *109*, 9529−9534. (f) Seth, R.; Discolo, C. M.; Palczewska, G. M.; Lewandowski, J. J.; Krakovitz, P. R. Ultrasound characterization of middle ear effusion. *Am. J. Otolaryngol.* **2013**, *34*, 44−50.

(9) (a) Carr, J. A.; Valdez, T. A.; Bruns, O. T.; Bawendi, M. G. Using the shortwave infrared to image middle ear pathologies. *Proc. Natl. Acad. Sci. U. S. A.* **2016**, *113*, 9989−9994. (b) Singh, S. P.; Xia, A.; Tusty, M.; Victorovich Malkovskiy, A.; Easwaran, M.; Zarabanda, D.; Valdez, T. A. Identification of early inflammatory changes in the tympanic membrane with Raman spectroscopy. *The Analyst* **2019**, *144*, 6721−6728. (c) Valdez, T. A.; Pandey, R.; Spegazzini, N.; Longo, K.; Roehm, C.; Dasari, R. R.; Barman, I. Multiwavelength fluorescence otoscope for video-rate chemical imaging of middle ear pathology. *Anal. Chem.* **2014**, *86*, 10454−10460. (d) Valdez, T. A.; Spegazzini, N.; Pandey, R.; Longo, K.; Grindle, C.; Peterson, D.; Barman, I. Multi-color reflectance imaging of middle ear pathology in vivo. *Anal. Bioanal. Chem.* **2015**, *407*, 3277−3283.

(10) Valdez, T. A.; Carr, J. A.; Kavanagh, K. R.; Schwartz, M.; Blake, D.; Bruns, O.; Bawendi, M. Initial findings of shortwave infrared otoscopy in a pediatric population. *Int. J. Pediatr. Otorhinolaryngol.* **2018**, *114*, 15−19.

(11) (a) Bruns, O. T.; Bischof, T. S.; Harris, D. K.; Franke, D.; Shi, Y.; Riedemann, L.; Bartelt, A.; Jaworski, F. B.; Carr, J. A.; Rowlands, C. J.; Wilson, M. W. B.; Chen, O.; Wei, H.; Hwang, G. W.; Montana, D. M.; Coropceanu, I.; Achorn, O. B.; Kloepper, J.; Heeren, J.; So, P. T. C.; Fukumura, D.; Jensen, K. F.; Jain, R. K.; Bawendi, M. G. Next-generation in vivo optical imaging with short-wave infrared quantum dots. *Nat. Biomed. Eng.* **2017**, *1*, 1−11. (b) Hong, G.; Diao, S.; Chang, J.; Antaris, A. L.; Chen, C.; Zhang, B.; Zhao, S.; Atochin, D. N.; Huang, P. L.; Andreasson, K. I.; Kuo, C. J.; Dai, H. Through-skull fluorescence imaging of the brain in a new near-infrared window. *Nat. Photonics* **2014**, *8*, 723−730. (c) Hong, G.; Lee, J. C.; Robinson, J. T.; Raaz, U.; Xie, L.; Huang, N. F.; Cooke, J. P.; Dai, H. Multifunctional in vivo vascular imaging using near-infrared II fluorescence. *Nat. Med.*

2012, *18*, 1841−1846. (d) Sordillo, L. A.; Pu, Y.; Pratavieira, S.; Budansky, Y.; Alfano, R. R. Deep optical imaging of tissue using the second and third near-infrared spectral windows. *J. Biomed. Opt.* **2014**, *19*, No. 056004.

(12) (a) Hamaguchi, Y.; Sakakura, Y.; Majima, Y.; Juhn, S. K. Kinetics of lysosomal protease activity in human otitis media with effusion. *Am. J. Otolaryngol.* **1987**, *8*, 194−198. (b) Hansen, T.; Unger, R. E.; Gaumann, A.; Hundorf, I.; Maurer, J.; Kirkpatrick, C. J.; Kriegsmann, J. Expression of matrix-degrading cysteine proteinase cathepsin K in cholesteatoma. *Mod. Pathol.* **2001**, *14*, 1226−1231.

(13) (a) Yim, J. J.; Tholen, M.; Klaassen, A.; Sorger, J.; Bogyo, M. Optimization of a Protease Activated Probe for Optical Surgical Navigation. *Mol. Pharmaceutics* **2018**, *15*, 750−758. (b) Ofori, L. O.; Withana, N. P.; Prestwood, T. R.; Verdoes, M.; Brady, J. J.; Winslow, M. M.; Sorger, J.; Bogyo, M. Design of Protease Activated Optical Contrast Agents That Exploit a Latent Lysosomotropic Effect for Use in Fluorescence-Guided Surgery. *ACS Chem. Biol.* **2015**, *10*, 1977−1988.

(14) Kariya, S.; Okano, M.; Aoji, K.; Kosaka, M.; Chikumoto, E.; Hattori, H.; Yuen, K.; Nishioka, S.; Nishioka, K.; Nishizaki, K. Role of macrophage migration inhibitory factor in otitis media with effusion in adults. *Clin. Diagn. Lab. Immunol.* **2003**, *10*, 417−422.

(15) (a) Wu, T. T.; Chen, T. L.; Chen, R. M. Lipopolysaccharide triggers macrophage activation of inflammatory cytokine expression, chemotaxis, phagocytosis, and oxidative ability via a toll-like receptor 4-dependent pathway: validated by RNA interference. *Toxicol. Lett.* **2009**, *191*, 195−202. (b) Zhang, J.; Chen, S.; Hou, Z.; Cai, J.; Dong, M.; Shi, X. Lipopolysaccharide-induced middle ear inflammation disrupts the cochlear intra-strial fluid-blood barrier through down-regulation of tight junction proteins. *PLoS One* **2015**, *10*, No. e0122572. (c) Buckiová, D.; Ranjan, S.; Newman, T. A.; Johnston, A. H.; Sood, R.; Kinnunen, P. K. J.; Popelář, J.; Chumak, T.; Syka, J. Minimally invasive drug delivery to the cochlea through application of nanoparticles to the round window membrane. *Nanomedicine* **2012**, *7*, 1339−1354. (d) Erickson, M. A.; Hansen, K.; Banks, W. A. Inflammation-induced dysfunction of the low-density lipoprotein receptor-related protein-1 at the blood-brain barrier: protection by the antioxidant N-acetylcysteine. *Brain, Behav., Immun.* **2012**, *26*, 1085−1094. (e) Hirose, K.; Li, S. Z.; Ohlemiller, K. K.; Ransohoff, R. M. Systemic lipopolysaccharide induces cochlear inflammation and exacerbates the synergistic ototoxicity of kanamycin and furosemide. *J. Assoc. Res. Otolaryngol.* **2014**, *15*, 555−570.

(16) (a) Hermansson, A.; Prellner, K.; Hellstrom, S. Persistent structural changes in the middle ear mucosa of the rat, after an experimentally induced episode of pneumococcal otitis media. *Acta Oto-Laryngol.* **1990**, *109*, 421−430. (b) Magnuson, K.; Hermansson, A.; Hellstrom, S. Healing of tympanic membrane after myringotomy during Streptococcus pneumoniae otitis media. An otomicroscopic and histologic study in the rat. *Ann. Otol., Rhinol., Laryngol.* **1996**, *105*, 397−404. (c) von Unge, M.; Bagger-Sjoback, D. Tympanic membrane changes in experimental otitis media with effusion. *Am. J. Otol.* **1994**, *15*, 663−669.

(17) Bashkatov, A. N.; Genina, E. A.; Kochubey, V. I.; Tuchin, V. V. Optical properties of human skin, subcutaneous and mucous tissues in the wavelength range from 400 to 2000 nm. *J. Phys. D: Appl. Phys.* **2005**, *38*, 2543−2555.

(18) Carr, J. A.; Franke, D.; Caram, J. R.; Perkinson, C. F.; Saif, M.; Askoxylakis, V.; Datta, M.; Fukumura, D.; Jain, R. K.; Bawendi, M. G.; Bruns, O. T. Shortwave infrared fluorescence imaging with the clinically approved near-infrared dye indocyanine green. *Proc. Natl. Acad. Sci. U. S. A.* **2018**, *115*, 4465−4470.

https://dx.doi.org/10.1021/acssensors.0c01272
ACS Sens. 2020, 5, 3411−3419